Pediatr Radiol (2011) 41:1085–1099
DOI 10.1007/s00247-011-2128-x

REVIEW

Imaging of pediatric ovarian neoplasms

Monica Epelman · Kudakwashe R. Chikwava · Nancy Chauvin · Sabah Servaes

Received: 26 January 2011 / Revised: 3 April 2011 / Accepted: 8 April 2011 / Published online: 13 May 2011

Abstract We review the clinical and imaging characteristics of the most common ovarian neoplasms in children and adolescents. Because of the widespread use of diagnostic imaging, incidental ovarian neoplasms might be encountered during the evaluation of abdominal pain, trauma or other indications and might pose a diagnostic dilemma. Conducting adequate imaging studies under these conditions is important, as management strategies differ according to the size and appearance of the lesion as well as the age of the patient. US dominates in gynecological imaging because of its excellent visualization, absence of ionizing radiation and sedation risks and comparatively low cost. For further examination of indeterminate lesions found using US, MRI is being used more progressively in this field, particularly for the evaluation of complex pelvic masses with the aim of distinguishing benign and malignant conditions and conditions requiring surgical intervention. CT is reserved primarily for tumor staging and follow-up and for emergency situations.

CME activity This article has been selected as the CME activity for the current month. Please visit the SPR website at www.pedrad.org on the Education page and follow the instructions to complete this CME activity.

M. Epelman (✉) · N. Chauvin · S. Servaes
Department of Radiology,
The Children's Hospital of Philadelphia,
34th Street and Civic Center Boulevard,
Philadelphia, PA 19104, USA
e-mail: monica_epelman@hotmail.com

K. R. Chikwava
Department of Pathology and Laboratory Medicine,
The Children's Hospital of Philadelphia,
University of Pennsylvania,
Philadelphia, PA, USA

Keywords Ovary · Masses · Neoplasms · Imaging · Children

Introduction

Although malignant ovarian neoplasms in girls are uncommon and account for less than 2% of all pediatric cancers [1–4], Pomeranz and Sabnis [5] reported that hospital admissions for ovarian masses overall represented approximately one-fifth as many emergency department admissions as did appendicitis during the same study period. In a retrospective 14-year review of 240 patients presenting at the Children's Hospital of Philadelphia [6] with 251 ovarian masses, it was found that nearly half of the lesions (48.8%) were neoplastic in etiology. Brookfield and co-workers [3] reported an incidence for malignant ovarian tumors of 0.102 per 100,000 girls per year in girls age 9 years or younger, with a 10-fold increase in girls age 10–19 years, to 1,072 per 100,000 girls per year. The same study also demonstrated that it is extraordinarily uncommon for infants younger than 1 year to have a malignant ovarian neoplasm. However, a higher index of suspicion for malignancy is needed in girls age 1 to 8 years, particularly in those presenting with a chief complaint of an abdominal mass or precocious puberty [3, 7], as malignancy can be found in approximately a quarter of these cases. In the 9–19 years age group, benign entities such as cysts or benign neoplasms are more common than malignant lesions, and malignancy is found in only 10% of the cases [3, 7]. Although ovarian malignancies are uncommon in pediatric patients, they account for approximately 10–20% [2, 3, 8] of the cases presenting with an ovarian mass and result in a diagnostic dilemma.

Ovarian tumors are classified on the basis of their origin as germ cell, epithelial, sex cord stromal or miscellaneous

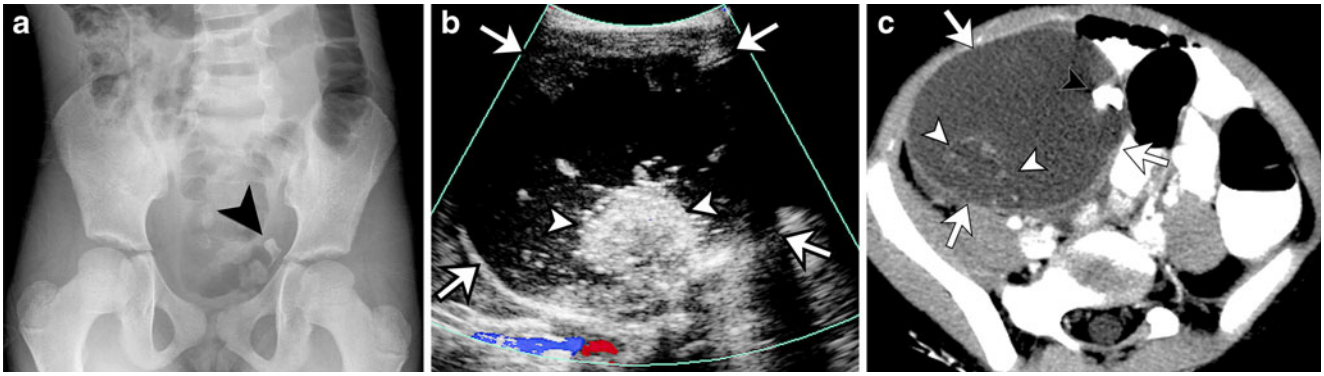

Fig. 1 Mature ovarian teratoma and dermoid plug in a 7-year-old girl with abdominal pain for 2 days, emesis and anorexia. Imaging studies were requested to evaluate for appendicitis. **a** Abdominal radiograph reveals a tooth-like calcific density (*black arrowhead*) indicating concern for a teratoma. **b** Characteristic US appearance of a mature ovarian teratoma (*white arrows*), which appears as a cystic adnexal lesion with an echogenic nodule (*white arrowheads*), frequently referred to as a dermoid plug or Rokitansky nodule. Note the multiple echogenic linear interfaces floating within the cyst representing hair fibers, which is known as the "dermoid mesh." **c** Corresponding axial CT image confirms the presence of the ovarian teratoma (*arrows*). The white arrowheads denote the dermoid plug or Rokitansky nodule. The *black arrowhead* points toward the tooth-like element. The ovary and tube were torsed at surgery

tumors. The histological distribution of these tumors in younger patients significantly differs from that in the adult population, and unlike the case in adults, in whom malignant tumors of epithelial origin represent approximately 95% of all ovarian malignancies, the most common ovarian neoplasms in females younger than 20 are of germ cell origin [3, 6, 9, 10], which represent nearly 80% of cases [3]. A recent 15-year review of 424 girls presenting with ovarian masses found that germ cell tumors constituted 50% of all pediatric ovarian malignancies, sex cord stromal tumors 28%, epithelial tumors 17% and other lesions 4% (ovarian involvement by leukemia and lymphoma) [7].

Children with germ cell and sex cord stromal tumors might exhibit acute abdominal pain as a presenting symptom, which is related to torsion, rupture and hemoperitoneum [11]. However, Oltmann et al. [12] recently reported that most ovarian torsions are not related to an underlying neoplasm acting as a lead point, and that there is specifically a very low incidence of malignant

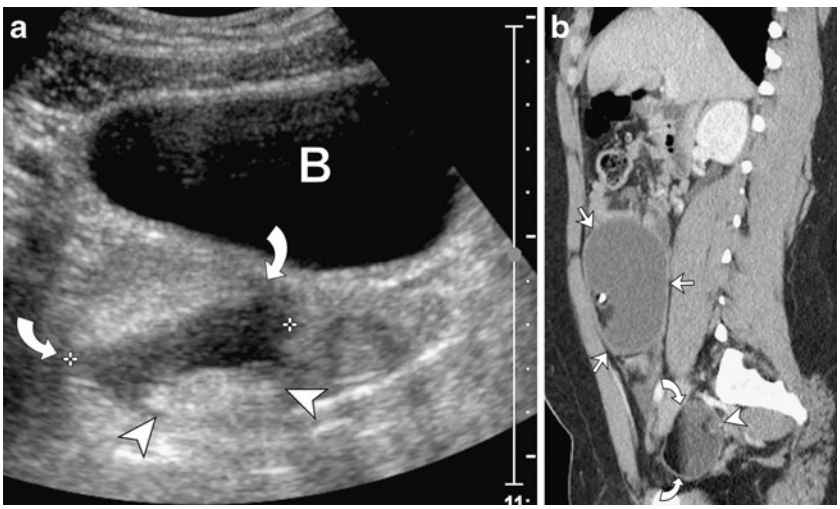

Fig. 2 Bilateral mature cystic teratomas showing fat-fluid levels in a 16-year-old with acute onset of left lower quadrant pain and emesis. On US a large left adnexal mass was seen (image not shown). **a** Parasagittal US scan through the right hemipelvis shows an additional 5-cm right adnexal lesion (*between calipers*) with a fat-fluid level (*curved arrows*) and a Rokintansky nodule (*arrowheads*). **b** Sagittal reformatted CT image confirms the appearance of bilateral mature teratomas. Note the fat-fluid level (*curved arrows*) and the Rokitansky nodule (*arrowhead*) corresponding with the US image. The *arrows* denote a large additional teratoma, which is relatively high and midline in position, a finding that should raise concern for ovarian torsion. At surgery a left ovarian torsion was detorsed. The bilateral ovarian masses were resected and bilateral partial oophorectomies were performed

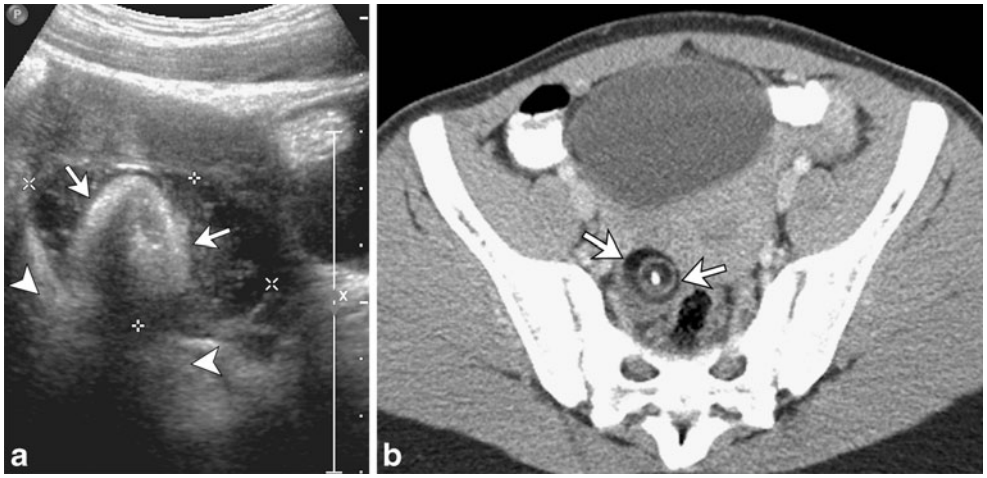

Fig. 3 A mature ovarian teratoma and "tip of the iceberg" sign in a 13-year-old girl. **a** Magnified transabdominal pelvic US image of the right ovary (*between calipers*) shows an echogenic adnexal mass (*arrows*) with posterior acoustic shadowing (*arrowheads*) consistent with a mature teratoma. The multitude of interfaces in the near field resulting from the mixture of fat and hair obscures the remainder of the lesion, and therefore the term "tip of the iceberg" is commonly used to denote this sign. **b** Corresponding axial CT image demonstrates a large amount of fatty tissue within the mass (*arrows*), a characteristic feature of mature ovarian teratomas

ovarian tumors presenting with torsion. The likelihood of malignancy is actually greater for patients presenting with a chief complaint of an abdominal mass or precocious puberty [7].

Abnormal hormonal activity, such as isosexual precocious puberty, has been classically associated with estrogen secretion in juvenile granulosa cell tumors, whereas masculinization has been related to Sertoli-Leydig cell tumors as a result of androgen secretion [7, 13]. Increased serum levels of beta human chorionic gonadotrophin (β-HCG) and α-fetoprotein (α-FP) are virtually diagnostic for malignant ovarian germ cell tumors when positive, although diagnosis is inconclusive if negative [7, 14, 15], as they might be positive in only 50% of the cases [7]. Subsequent monitoring of β-HCG and α-FP can be used to monitor for early relapse. Increased preoperative levels of CA 125 are associated with poor prognosis [16] and are most commonly found in association with epithelial cell tumors [6]. Elevated serum LDH (lactic dehydrogenase) levels have been more specifically associated with dysgerminoma [17], while elevated α-FP levels are commonly seen in yolk sac and Sertoli-Leydig cell tumors. Imaging findings thought to be associated with a higher risk of malignancy include a solid or a heterogeneous appearance versus a cystic appearance, which is considered more reassuring for benign lesions, although cystic lesions harbor malignant cells in nearly 5% of cases [7]. Unlike in adults, in whom lesions greater than 4 cm are considered suspicious for harboring malignancy [18], in children, ovarian masses are worrisome for malignancy if they are

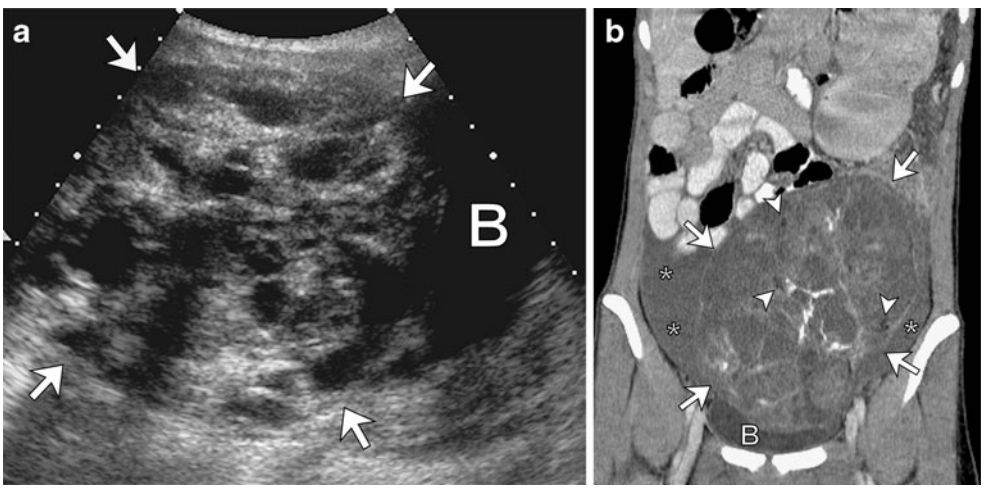

Fig. 4 Immature ovarian teratoma in 16-year-old previously healthy girl who noted an increasing abdominal girth coincident with increasing lower abdominal pain with activities over approximately 3 months. **a** US shows a large, complex midline mass (*arrows*). **b** Coronal reformatted CT image shows a large immature ovarian teratoma (*arrows*) with a scant amount of fat (*arrowheads*) and a few foci of calcification. Note the moderate amount of ascites (*asterisks*). *B* = bladder

larger than 7.5–8.0 cm [7, 14, 19]. In general, most malignant tumors are responsive to chemotherapy and have an excellent prognosis with optimal therapy [20–22].

Germ cell tumors

Ovarian germ cell tumors constitute the most common type of ovarian neoplasms in childhood and adolescence [11]. The most common presenting symptom for these tumors is abdominal pain, followed by abdominal distention and a palpable mass [20]. The histological subtypes of germ cell tumors according to the World Health Organization (WHO) include teratoma (mature, immature and mixed); dysgerminoma; endodermal sinus tumor, also called yolk sac tumors; embryonal carcinoma; polyembrioma; and ovarian non-gestational choriocarcinoma [11]. Among malignant lesions, malignant teratomas are the most common histological subtype, constituting 38.5% of cases, followed by dysgerminoma, representing nearly 33%, and nondysgerminoma or mixed cell types, comprising approximately 28% of cases [22]. Among these, embryonal carcinomas, ovarian chorio-

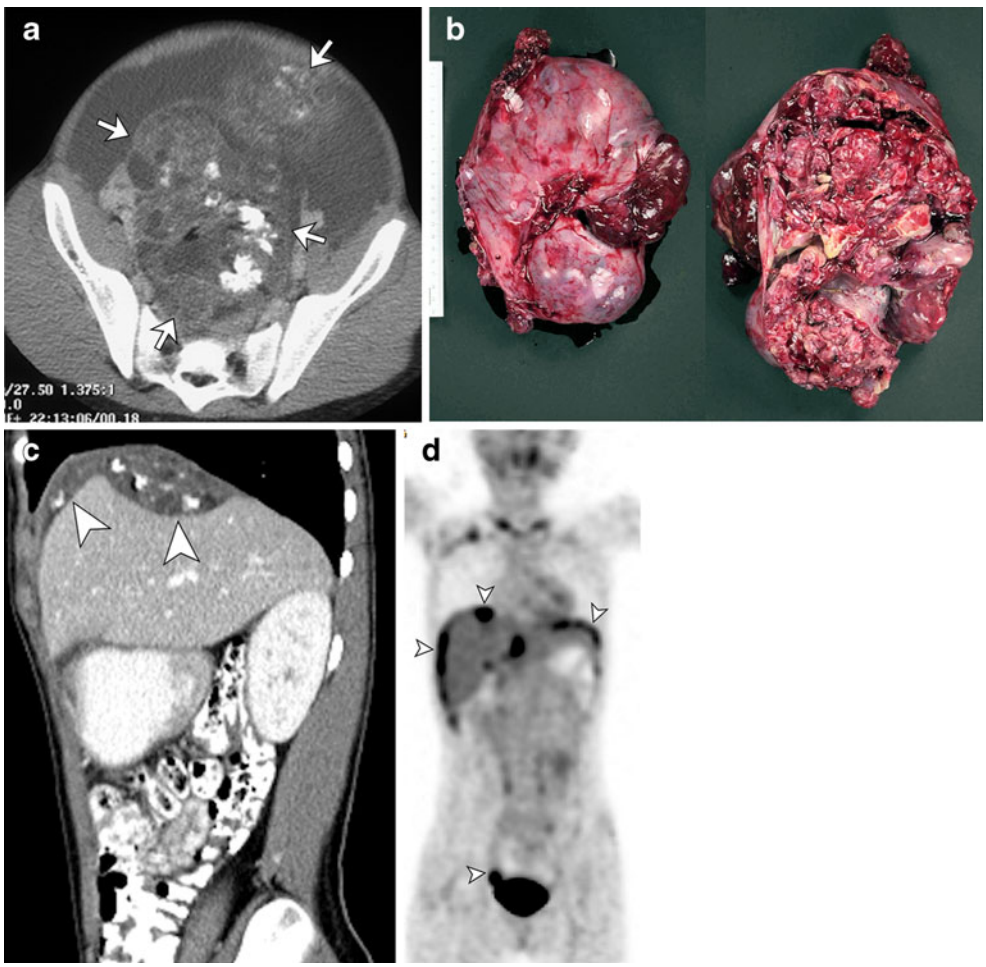

Fig. 5 Growing teratoma syndrome in an 11-year-old following bilateral oophorectomies for bilateral, large immature teratomas. **a** Initial enhanced axial CT scan after a 2-week history of increasing abdominal girth, decreased appetite and fatigue shows large, complex abdominal masses with calcified and scant fatty components. Based on pathology results, it was discovered that she had both immature and mature components of teratoma (*arrows*). Note the large amount of ascites. **b** Gross pathology images show a large 2,240-gram, 24×17×13-cm mass with a partially disrupted smooth surface from which hemorrhagic tissue is exuding. The cut surface reveals solid areas composed of soft white-tan to red-tan gelatinous tissue, innumerable small cystic spaces and white-tan calcified areas consistent with bone or dental structures. **c** Sagittal reformatted CT and (**d**) coronal PET images obtained following 4 weeks of chemotherapy reveal what appears to be recurrent intraperitoneal disease, most pronounced within the right upper quadrant (*arrowheads*) and deep pelvis (image not shown), with extensive peritoneal implants but with better-defined cystic, fatty and calcific densities compared to initial scans. These foci were metabolically active on a PET scan (*arrowheads*). However, at this time, the girl had a normal α-fetoprotein level. This incongruence prompted a second look surgery for resectioning and tissue analysis. The final pathology of the lesions removed demonstrated mature elements from all three germ layers, including bone, cartilage, respiratory epithelium, squamous epithelium, skin, fat, fibrous tissue and mature neuroglial tissue consistent with gliomatosis peritonei. No immature or malignant elements were found

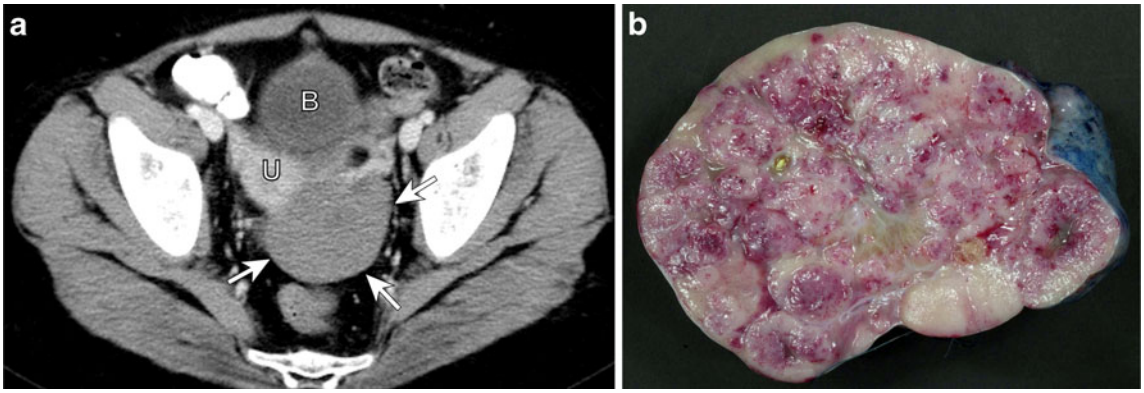

Fig. 6 Incidentally discovered dysgerminoma with coexistent gonadoblastoma in a 12-year-old girl with common variable immunodeficiency hyper IgM syndrome. **a** Axial CT image shows a relatively homogeneous enhancing soft-tissue mass (*arrows*) originating from the left adnexa. *B* = bladder, *U* = uterus. **b** The gross pathology specimen, a 658-gram and 14.5×11.5×7.8-cm tumor, shows a cut surface with homogeneously tan and slightly hemorrhagic nodules ranging from 0.5 to 3.5 cm

carcinoma and polyembrioma are the least common types and usually present in a pure form in unusual cases [22]. Malignant germ cell tumors metastasize to the lungs, liver and peritoneum [23]. Children with gonadal dysgenesis are at increased risk for the development of germ cell tumors [24].

Mature cystic teratoma is the most common type of ovarian neoplasm in children [25] and the only benign form. At least two of the three germ cell layers, the ectoderm, mesoderm or endoderm, are present in these tumors [25]. Mature cystic teratomas are known for containing hair, muscle, teeth, bone and skin lining the wall and predominating at the Rokitansky nodule under pathological examination. Mature cystic teratomas are commonly called dermoid cysts because of the preponder-

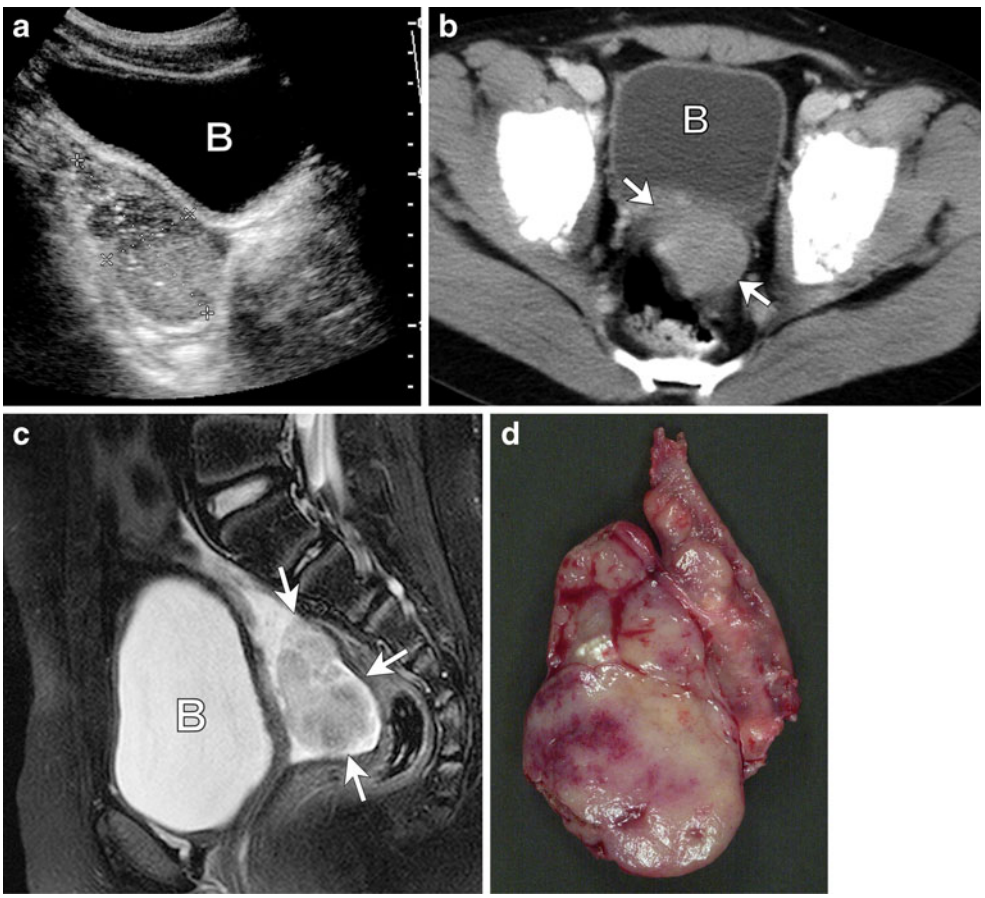

Fig. 7 Dysgerminoma with coexistent mature teratoma in a patient with Frasier syndrome, a condition characterized by gonadal dysgenesis, progressive glomerulopathy and a mutation in the Wilms tumor gene (WT1 gene). **a** Sagittal US scan through the pelvis shows a solid adnexal mass (*between calipers*). **b** The mass (*arrows*) shows relatively homogeneous enhancement under axial CT. **c** Sagittal T2-W MRI reveals a lobulated, high T2 signal lesion (*arrows*). Note that no uterus is identified in this midline scan, an expected finding in this patient with Frasier syndrome. **d** The gross pathology specimen shows a tan, fleshy nodular tumor, 33.3 g and 6.5×5×2.5 cm, with focal areas of reddish discoloration. No cysts are identified. *B* = bladder

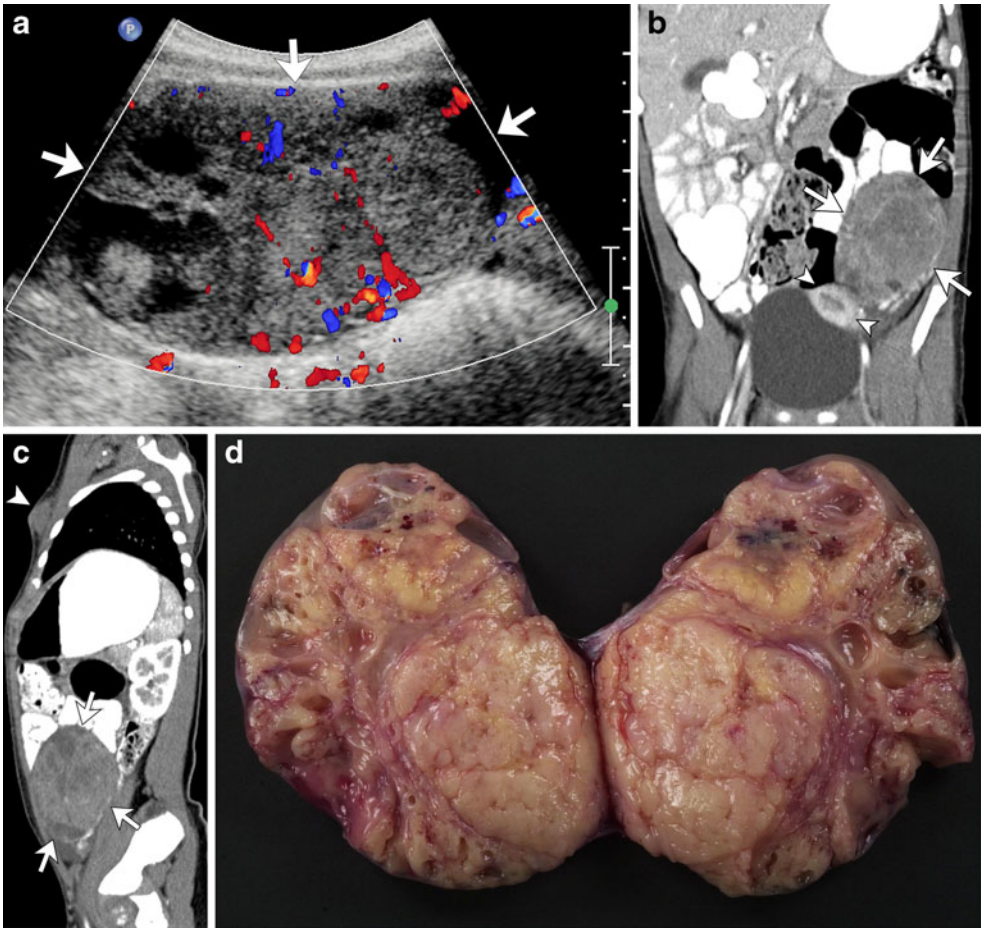

Fig. 8 Juvenile granulosa cell tumor in a 3-year-old girl with precocious puberty. **a** Large, complex, heterogeneous mass is seen with US, with solid and cystic components (*arrows*). Increased flow is noted within the solid components on color Doppler interrogation. **b** Coronal reformatted CT image shows the complex appearance of the left ovarian mass (*arrows*). Note the pubertal appearance of the uterus (*arrowheads*). **c** Sagittal reformatted CT image shows the complex mass in the left lower quadrant (*arrows*). Note the presence of breast buds (*arrowhead*) in this patient with premature telarche. **d** The gross specimen consists of a pink-tan mass, 188 g, 9×7×4.5 cm. Cut surfaces reveal yellow-tan tissue with multiple cystic cavities, 2.5 cm in greatest dimension, containing straw-colored serous fluid

ance of ectodermal elements. Because of their various components, mature teratomas vary in appearance, particularly on US. The size of the dermoid plug and the magnitude and location of the calcified elements, as well as the composition of the fatty components, are considered the determining factors for this variable appearance [26]. Most frequently, they manifest as a unilocular cystic lesion, with a hyperechoic nodule protruding into the cyst lumen, the so-called Rokitansky nodule or dermoid plug (Fig. 1). This contains hair follicles and often fragments of bone or teeth. The "dermoid mesh" (Fig. 1) refers to multiple echogenic linear interfaces, representing hair fibers, that might be seen floating within the cyst [26–29]. A fat–fluid interface is a distinguishing feature of mature teratomas and it is related to the presence of echogenic sebum floating above hypoechoic serous fluid (Fig. 2) [25]. The "tip of the iceberg" sign (Fig. 3) refers to the US appearance of the dermoid plug as an echogenic mass in the near-field resulting in posterior shadowing that makes visualization of the bulk of the lesion difficult and hides the posterior wall of the cyst. Care should be taken not to confuse an echogenic loop of bowel for a diffusely echogenic mature teratoma and vice versa [25]. Conversely, on CT and MRI the appearance of mature teratomas is nearly pathognomonic and is characterized by the presence of intratumoral fat consisting of adipose tissue within the cyst wall or dermoid plug and of sebum within the cyst lumen [25]. The latter characteristic is the most specific imaging finding for the diagnosis of mature teratoma [30]. Fat presents a high

Fig. 9 Palpable abdominal mass in an 8-year-old girl. Enhanced axial CT image shows a large, multiloculated cystic mass (*arrows*) with enhancing septations and locules of varying sizes. Pathology was consistent with a juvenile granulosa cell tumor. The mass results in a bulge in the abdominal wall (*arrowhead*)

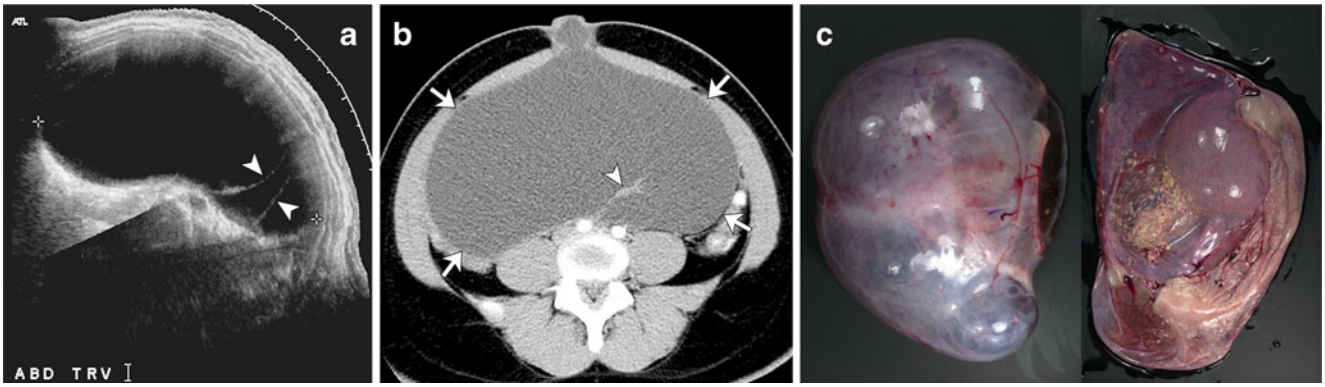

Fig. 10 Juvenile granulosa cell tumor in a 14-year-old girl with increasing abdominal distention. **a** Transverse US scan through the abdomen shows a simple-appearing cystic lesion (*between calipers*) with a few thin septations (*arrowheads*). **b** Enhanced axial CT image shows a massive cystic mass with a simple appearance (*arrows*) and a few septations (*arrowhead*) that proved to be a juvenile granulosa cell tumor based on pathology. The lesion measured 30×30 cm and spanned from pelvis to the upper abdomen. Note how the mass herniates through the umbilicus. **c** Gross pathology specimen shows an irregular 5,600-gram and 34×22×10-cm mass with a dark red smooth and glistening external surface

signal intensity on T1-weighted sequences that is suppressed when utilizing fat-saturation sequences. Conversely, the high T1 signal of blood-related products or proteinaceous contents does not suppress on fat-saturation imaging. The presence of calcific components within the Rokitansky nodule facilitates the diagnosis of mature teratomas, particularly on CT scans because of their characteristic appearance in this modality [31–33].

The reported complications of ovarian teratomas include torsion, which is seen in nearly 15% of all cases; rupture; infection; malignant transformation and infrequently autoimmune hemolytic anemia and immune-mediated limbic encephalitis [28, 32, 34].

Immature teratomas typically affect a younger age group and have a worse prognosis [32]. These are classified according to their level of differentiation; because the most constant component is neural tissue, the level of malignancy is determined by the proportion and degree of neuroectodermal tissue differentiation. As stated previously, elevated pre-operative levels of β-HCG and α-FP are nearly diagnostic of malignant ovarian germ cell tumors; however, these might be present in only 50% of cases [7]. Subsequent monitoring of β-HCG and α-FP is generally utilized for relapse surveillance. With imaging, immature teratomas are usually larger and demonstrate prominent areas of soft tissue, scattered foci of fat and fewer calcifications (Figs. 4 and 5) [32]. According to Alotaibi and Navarro [35], the preponderance of a cystic component with variable amounts of fat and calcification favors the diagnosis of a mature teratoma, while a predominantly solid appearance with scattered foci of fat and calcification favors the diagnosis of immature types. Recently, Vaysse et al. [19] proposed a 7.5-cm cutoff

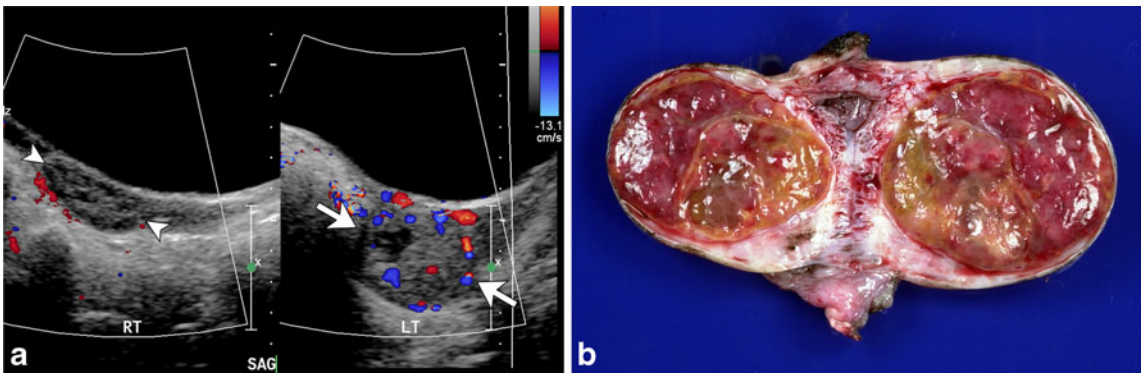

Fig. 11 Sertoli-Leydig tumor in a 13-year-old with rapidly progressive virilization symptoms consisting of primary amenorrhea, acne, deepening of the voice and increased facial hair. **a** Sagittal US scan through the pelvis reveals a relatively enlarged and hyperemic left ovary (*arrows*) compared to the right (*arrowheads*). **b** The gross specimen shows a red-tan to orange-tan solid tumor, 4.8 cm in greatest dimension, replacing the ovarian parenchyma. The capsule is intact. Microscopic evaluation revealed Sertoli-Leydig tumor with no evidence of capsular invasion or heterologous/sarcomatous elements within the mass

size as an important criterion to differentiate preoperatively between benign and malignant neoplasms. Mature teratomas might be found in 10% of patients with contralateral immature neoplasms; Therefore bilateral involvement does not necessarily infer a malignant process [21].

Growing teratoma syndrome is an uncommon phenomenon that follows successful treatment of malignant nonseminomatous germ-cell tumors. Its incidence in children with immature teratomas has been reported to be as high as 30% [20]. It is characterized by the appearance of secondary masses that histologically consist of benign cells. Although the development of new or enlarging masses following treatment is considered recurrence of malignancy, this is not the case with a growing teratoma. These masses usually demonstrate better defined margins, increased density and foci of calcification. They characteristically initiate at the site of the original lesion and extend into remote locations. Recognition of this phenomenon is important to prevent confusion with tumor progression (Fig. 5) [28, 36, 37].

Dysgerminomas are the least differentiated type of germ cell tumors and are equivalent to seminomas in males. These tumors, whether pure or combined with other elements, are the most common form of malignant ovarian neoplasm mainly affecting adolescents and young girls. With imaging, they appear as a solid, lobulated mass because of their internal architecture, which exhibits thin fibrovascular septa that typically enhance following the administration of an intravenous contrast agent in MR imaging. It is not uncommon to observe calcifications or small cysts within these lesions, which might be the result of necrosis and hemorrhage [34, 38]. Bilateral involvement occurs in approximately 10–15% of these cases. Unlike other ovarian tumors, dysgerminomas are highly radiosensitive and pelvic and retroperitoneal lymph node spreading is more frequent than intraperitoneal seeding. The correlation of these tumors with elevated laboratory values of LDH helps support their diagnosis [4, 17, 21]. It is not uncommon for dysgerminomas to be found in combination with other germ cell tumors (Fig. 6). This is particularly true in cases of gonadal dysgenesis, in which they are commonly found in association with gonadoblastoma (Fig. 7) [21, 24].

Sex cord stromal neoplasms

Sex cord stromal neoplasms originate from nongerminative tissue and arise from sex-cord-derived cells (granulosa cells in the normal ovary, Sertoli cells in the testis and Sertoli cells in ovarian tumors) and ovarian stromal cells (fibroblasts, theca cells and Leydig cells) [39]. Although several histological types are found in this group, two main groups are commonly considered, the granulosa-theca cell tumors and the Sertoli-Leydig cell tumors. Sex cord stromal neoplasms are usually hormonally active and are classically associated either with isosexual precocious puberty (juvenile granulosa cell tumor), or virilization and hirsutism (Sertoli-Leydig cell tumors). However, Cecchetto and coworkers [40] recently reported that signs of abnormal hormonal secretion were found in only 9 out of 23 patients and that the most common presenting symptom was abdominal pain, with or without an associated abdominal mass. This is probably related to the increasing use of imaging, thus permitting early diagnosis and treatment.

Granulosa cell tumor types are the most common malignant sex cord stromal neoplasm. Granulosa cell tumors are unusual in the pediatric population, with the

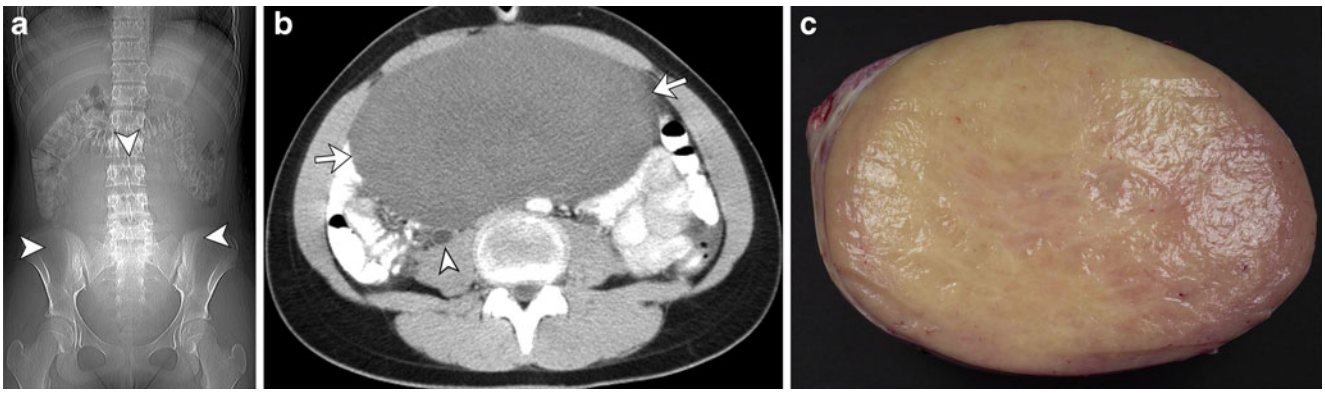

Fig. 12 Fibrothecoma in a 13-year-old girl who presented to the emergency department with abdominal fullness and pain. **a** Scout view of the abdomen shows a mass (*arrowheads*) displacing the bowel loops. **b** Axial enhanced CT of the abdomen demonstrates a relatively homogeneous mass (*arrows*) with mild enhancement. Note the right hydroureter (*arrowhead*) resulting from compression by the mass. **c** Gross pathology specimen shows a firm, 115.7-gram, 7×5.3×4.5-cm, mass that has been sectioned to reveal uniformly pale tan to white, whorled parenchyma

exception of juvenile granulosa cell tumors (JGCTs). JGCTs exhibit less aggressive behavior than that of the adult type and typically affect prepubescent girls. They are often associated with isosexual pseudoprecocity, presenting with breast and labial enlargement, pubic and axillary hair and vaginal discharge [41, 42]. These physical changes are related to the hyperestrogenic state induced by tumor secretion (estradiol secretion in hormonally active tumors). Postpubertal patients with hormonally active JGCTs might develop menstrual irregularities, menorrhagia, intermenstrual bleeding or amenorrhea [42]. JGCTs are usually unilateral in presentation and can reach large sizes. Most cases, approximately 90%, are diagnosed in early stages of disease and have a favorable prognosis [42–44]. Inhibin is the tumor marker used to monitor these lesions [42]. JGCTs have been associated with Ollier disease and Maffucci syndrome [39] and should be strongly considered in the differential diagnosis of young patients with these conditions presenting with an ovarian neoplasm. Under gross examination, the majority of JGCTs present with solid and cystic components. Both solid and cystic portions might contain associated hemorrhagic products [41]. Under microscopic examination, focal follicle formation is a typical feature, which might explain the multicystic appearance on imaging. Regarding imaging, granulosa cell tumors vary widely. Granulosa cell tumors present with a

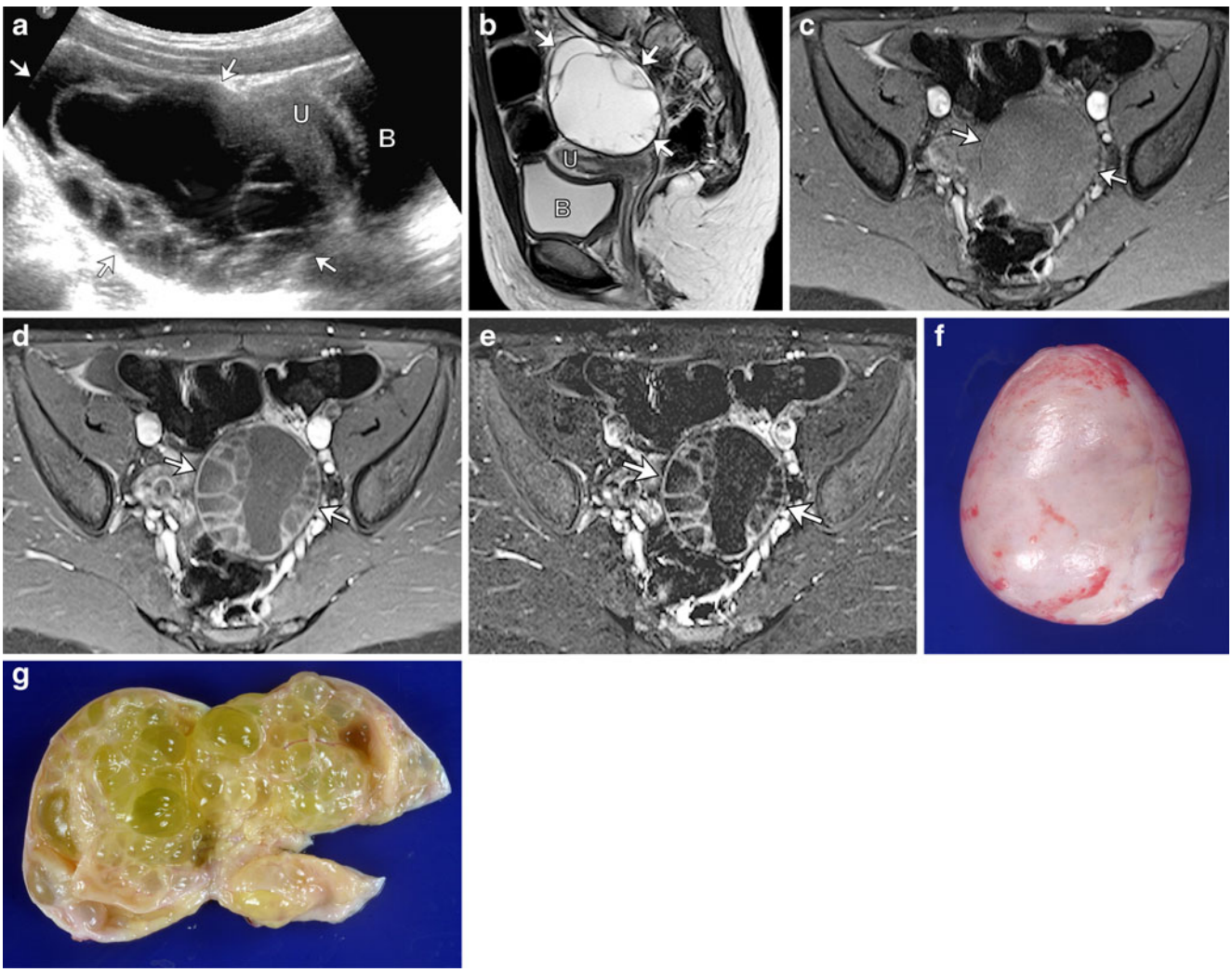

Fig. 13 Sex cord tumor with annular tubules in a 6-year-old girl with precocious puberty. **a** Sagittal scan through the pelvis reveals an enlarged ovary with multiple cysts of varying sizes (*arrows*). **b** Sagittal T2-W MRI reveals a multicystic lesion with some T2-shading and a few hypointense foci reflective of blood products. **c-e** Axial substraction MR images show marked enhancement of their septa resulting in a spongy appearance (**c**, unenhanced; **d**, gadolinium-enhanced; **e**, substracted). Note the pubertal appearance of the uterus (*U*) on US and MRI images. **f** The specimen consists of a 48.14 g, 5.5×5.0×3.0-cm cystic ovary. The capsular surface is tan-white and smooth. **g** The cut surface shows multiple small cysts, up to 1.2 cm in greatest dimension each, filled with clear serous or tan-yellow mucoid material. The cyst walls are 0.1-cm thick and the cyst lining is tan-white and smooth. *B* = bladder

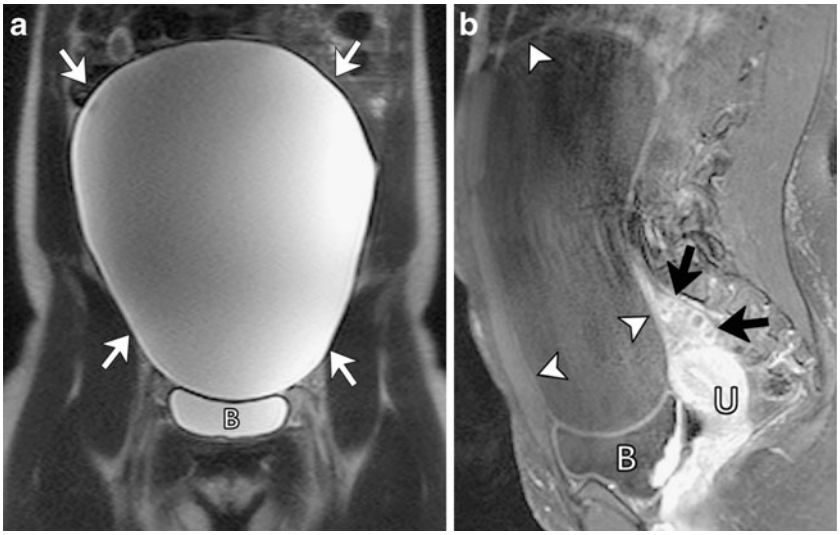

Fig. 14 Benign serous cystadenoma in a 15-year-old girl complaining of increasing abdominal distention for the last several months. **a** Coronal T2-W image reveals a large, thin-walled unilocular cystic mass (*white arrows*) extending from the pelvis into the upper abdomen measuring 22×19 cm. The lesion displaces the bowel superiorly. **b** Gadolinium-enhanced fat-suppressed T1-W MRI shows mild enhancement of the tumor thin wall (*arrowheads*) and demonstrates the relationship to residual ovarian tissue with a normal appearance (*black arrows*). The tumor causes a bulge in the abdominal wall. *B* = bladder, *U* = uterus

spectrum of imaging appearances related to their various histological appearances and different arrangements of tumor cells. They manifest as solid masses, as tumors with hemorrhagic or fibrotic changes (Fig. 8), as multilocular cystic lesions (Fig. 9) or as completely cystic neoplasms (Fig. 10) [45]. The heterogeneous appearance of their solid components is related to intratumoral bleeding, infarct, fibrous degeneration, and irregularly arranged tumor cells. Kim and Kim [46] categorized these neoplasms into two most common types: large multiseptated cystic masses, and medium solid masses with internal cystic components, which refers to single, well-defined solid lesions with internal cystic components. On MR imaging, specifically on T2-weighted sequences, these lesions exhibit a distinctive sponge-like appearance [39, 46, 47] associated with a solid lesion of intermediate signal and innumerable cystic spaces. Unusual presentations, including large unilocular cystic and entirely solid forms, have also been described [41, 46]. Intratumoral hemorrhagic products are a common finding in granulosa cell tumors and can be seen in as many as 70% of cases [46, 48]. Uterine changes such as uterine hyperplasia and endometrial thickening are not uncommon and are related to estrogenic effects [39, 45, 46].

Sertoli-Leydig cell tumors, formerly known as androblastomas or arrhenoblastomas, are classically associated with virilization. However, most of these neoplasms are

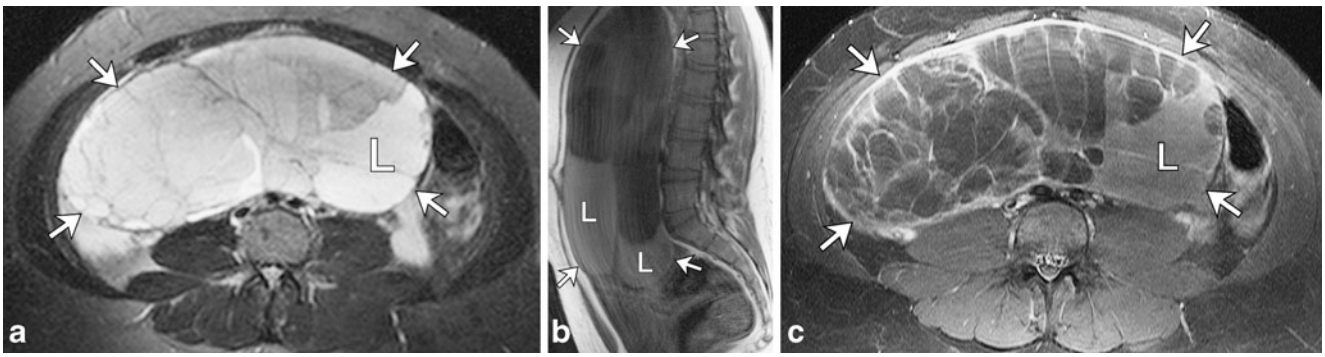

Fig. 15 Benign mucinous cystadenoma in an otherwise healthy 15-year-old presenting with a pelvic mass. **a** Axial T2-W fat-suppressed and **(b)** sagittal T1-W and MR images show a large, multilocular mass (*white arrows*) with a small, honeycomb-like configuration of the smaller locules characteristic of these types of lesions. Note T2 shading within some of the locules (*L*) on T2-W images that also demonstrate a high signal on T1-W images (*L* on **b**), reflecting blood products. **c** Post-gadolinium axial T1-W fat-suppressed image shows the mass (*arrows*) with enhancement of the septations and no significant enhancement of the locule (L)

nonfunctional and only 30–40% of all cases produce male hormones [40, 44, 45]. With US, these lesions appear as solid, predominantly hypoechoic lesions (Fig. 11), while on MRI they manifest as predominantly hypointense solid lesions on T2-weighted sequences, depending on their fibrous content. In some instances, these neoplasms are indistinguishable from granulosa cell tumors [34, 39].

Fibromas, thecomas or fibrothecomas and sclerosing stromal tumors are generally benign histotypes arising from the stromal elements of the ovaries. These tumors are infrequent and are even more unusual in the pediatric population [40]. Fibromas are rarely seen in patients younger than 40 years of age [39] and are classically associated with Meigs syndrome, ascites and right-side pleural effusion, which resolve following tumor resection. Thecomas and fibrothecomas are a spectrum of benign tumors with variable populations of both theca cells and fibroblasts [34, 39]. The theca cells account for the estrogenic effects of these neoplasms. Their US and MR imaging appearances are variable and depend on the amount of fibrous tissue, which typically demonstrates a low-signal on T1- and T2-weighted sequences [34, 39]. Additionally, tumors with a preponderance of fibrous tissue will demonstrate delayed, weak enhancement in dynamic contrast exams. With CT, fibrothecomas manifest as solid lesions with a variable degree of enhancement (Fig. 12). Calcifications may be present [49]. As these neoplasms increase in size, myxoid or cystic degeneration can occur, causing a heterogeneous appearance and less enhancement. A lack of enhancement of the neoplasm raises suspicion for ovarian torsion. Ascites has been reported in 30% to 82% of these patients [39, 49].

Other sex cord stromal tumors include sex cord tumor with annular tubules, sclerosing stromal tumors and gynandroblastoma. Sex cord tumor with annular tubules has morphological features of both granulosa cell and Sertoli cell tumors and might secrete estrogens, progesterone and a mullerian-inhibiting substance, which is used as a tumor marker of recurrence. Sex cord tumor with annular tubules is typically associated with Peutz-Jeghers syndrome, an autosomal-dominant condition caused by mutations in the SKT11 gene with loss of tumor suppressor activity. Individuals with this syndrome are at high risk for intestinal and extraintestinal malignancies, including pancreatic, breast and ovarian malignancies. When associated with Peutz-Jeghers syndrome, these tumors are usually small, tend to contain internal calcifications and can be bilateral. Conversely, patients with sex cord tumor with annular tubules in the absence of Peutz-Jeghers syndrome typically present with large, unilateral tumors (Fig. 13) [39, 50–52].

Epithelial neoplasms

Carcinomas account for approximately 95% of ovarian cancers in women of all ages, but they are extremely uncommon in pre-menarchal girls. Most epithelial neoplasms are serous, followed by other miscellaneous epithelial tumors, mucinous tumors, endometrioid tumors and clear cell tumors, in order of frequency. Each of these tumor types is further classified as benign, borderline or malignant, according to the clinical behavior of the tumor [53]. Serous and mucinous cystadenomas are the most common histological types in the pediatric age group, with serous types being more common than mucinous types [6]. These lesions initially manifest with torsion, particularly if their size ranges 8–10 cm. Surprisingly, torsion is not

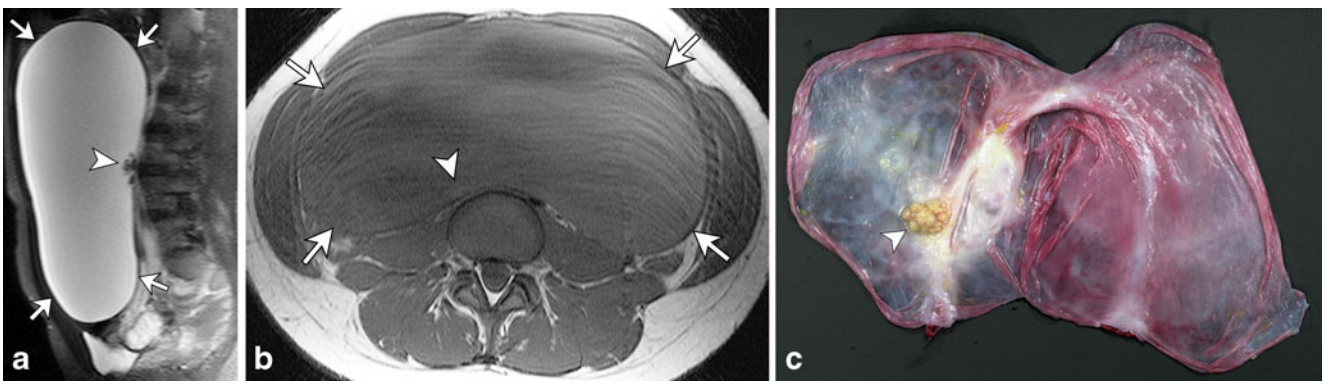

Fig. 16 Benign serous cystadenofibroma in a 19-year-old woman with increasing abdominal distention. **a** Sagittal T2-W and (**b**) axial T1-W MR images show an enormous unilocular cystic mass (*arrows*) with a focal cluster of low signal on T2-W images (*arrowhead*). The cluster is isointense on T1 (*arrowhead*) and barely identifiable from the fluid of the cyst. **c** Photograph of the gross specimen shows a 3×2×1-cm cluster of papillary projections (*arrowhead*) arising in the cyst, with otherwise smooth lining. The specimen, 3,460 g and 24.5×21.5×10 cm, contained approximately 600 mL of tan-yellow fluid. (Microscopic examination of the papillary projections showed abundant fibrous stroma)

associated with lesions larger than 15 cm [54]. Serous cystadenomas present as unilocular or multilocular cystic masses with homogeneous cystic components and thin septations (Fig. 14) but without papillary excrescences. Mucinous cystadenomas are typically large, multiloculated cystic masses with thin septations and locules that contain fluids of differing MRI signal intensities. The locules in these tumors are typically small and numerous (Fig. 15) [4, 54–56]. Serous cystadenofibromas are relatively rare, benign, epithelial-lined cystic lesions characterized by the presence of a solid fibrous stroma within the lesion. With MR imaging, this solid component typically manifests with a very low signal on T2-weighted sequences (Fig. 16) [57, 58].

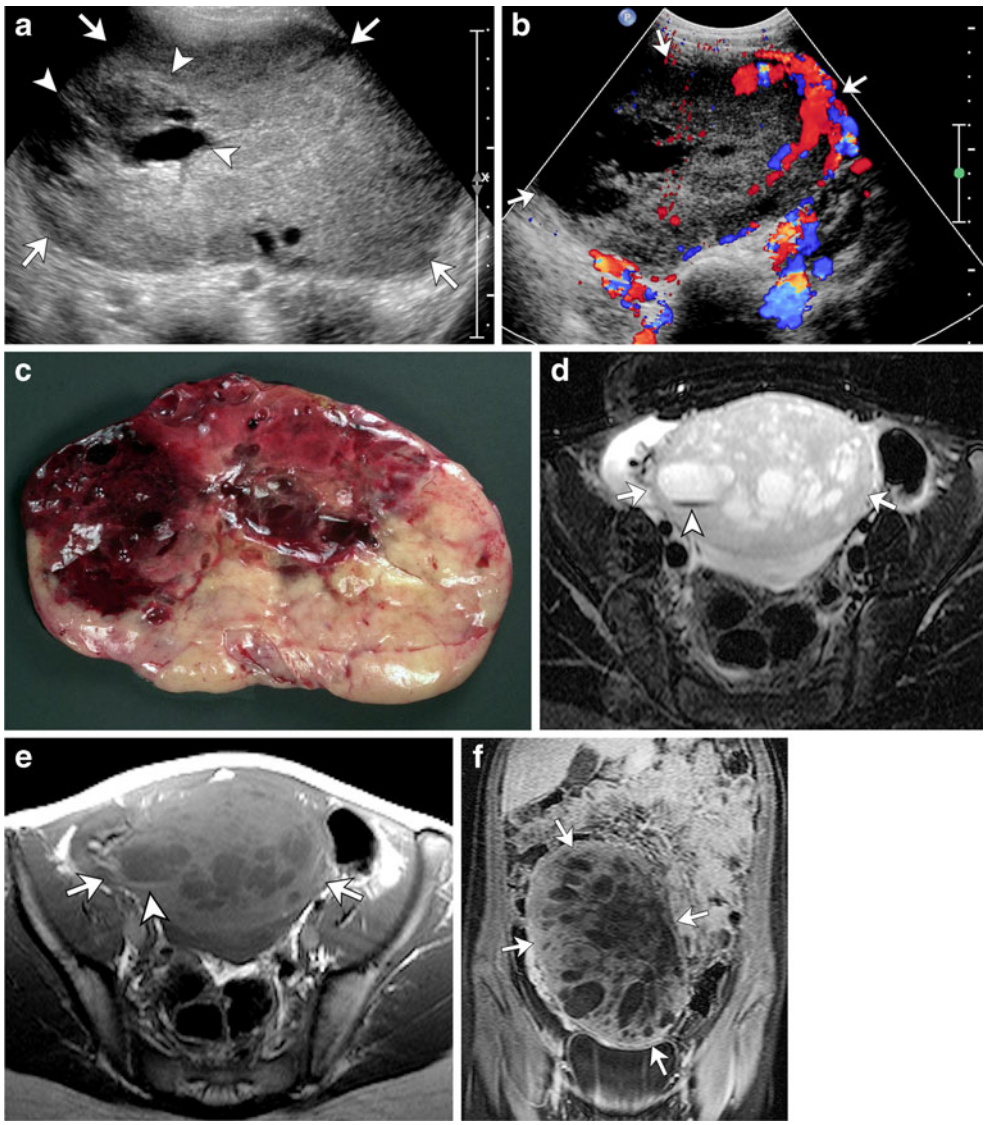

Fig. 17 Small cell carcinoma of the ovary in two patients. **a** Transverse US scan of the pelvis shows a predominantly solid, complex pelvic mass (*arrows*) in a 13-year-old girl presenting with lethargy and a calcium level of 18 mg/dL. Cystic changes (*arrowheads*) are noted in the right portion of the mass, corresponding to the necrotic changes seen in gross pathology. **b** Transverse color Doppler interrogation through the same mass (*arrows*) as (**a**) reveals a relative paucity of flow in this area, with relatively increased flow on the opposite side. Note the prominent vessels seen on the left side of the mass. **c** Gross pathology specimen shows a well-circumscribed, oval, 1,600-gram and 21×16×7.5-cm, predominantly solid lobulated mass with a tan-pink to red cut surface and with foci of cyst formation, hemorrhage and necrosis. The cysts range from 0.2 to 2.5 cm in maximum dimension with tan smooth walls and contain clear to hemorrhagic fluid. (Microscopic examination, together with clinical history, was consistent with small cell carcinoma, hypercalcemic type). **d** Axial T2-W and (**e**) axial T1-W MR images in an 11-year-old girl with the same type of tumor (*arrows*), small cell carcinoma of the hypercalcemic type with multiple fluid-fluid levels, some of which demonstrate low signal on T2 and high signal on T1, consistent with blood products (*arrowhead*). **f** Coronal T1-W fat-suppressed image following intravenous contrast administration shows heterogeneous enhancement of the mass (*arrows*) with multiple internal, unenhanced components reflecting necrosis

Miscellaneous lesions

Small cell carcinoma of the ovary is a rare and often lethal type of malignant tumor of the ovary primarily affecting young women between the ages of 9 and 43 years [59, 60]. In rare occasions these neoplasms are familial and possibly inherited [59, 60]. The cell lineage of this tumor type is unclear, and in the most recent WHO classification it was included in the group of miscellaneous tumors. These tumors are usually unilateral, with a propensity for intraabdominal spreading, and are frequently associated with paraendocrine hypercalcemia [61]. Their manifestations include fatigue, lethargy, polydypsia, and polyuria [62]. Other nonspecific clinical manifestations include abdominal pain and swelling, pelvic pain or mass [62]. Macroscopically, these neoplasms show predominantly solid tissue, with areas of hemorrhage or necrosis, and they are sometimes confounded with JGCT, even in their pathology [60]. These tumors are usually monitored through calcium levels. Therefore, in the concomitant presence of hypercalcemia and an ovarian mass in girls and adolescents, the diagnosis of small cell carcinoma of the ovary should be raised in the differential diagnosis (Fig. 17).

Metastatic spread to the ovary is rare in children, and unlike in adults, it usually occurs hematogenously. It is most commonly associated with mucinous adenocarcinoma of the colon, followed by Burkitt lymphoma, alveolar rhabdomyosarcoma, Wilms tumor, neuroblastoma, and retinoblastoma [63], in order of frequency. Bilateral involvement is encountered in as many as 56% of these patients [63]. Large or bilateral ovarian masses, which might be indistinguishable from the ovaries, should raise suspicion of an underlying malignancy elsewhere that has metastasized to the ovary. In these cases, the presence of metastatic foci on other organs provides a clue to the correct diagnosis. Burkitt-type non-Hodgkin lymphoma is an uncommon cause of ovarian masses; it has been described in pediatric patients, particularly in association with HIV/AIDS. Imaging in these cases might reveal solid lesions with small peripheral follicles (Fig. 18). Recognition of this entity is important, as management differs in such patients in whom chemotherapy is the initial treatment of choice [64, 65].

Conclusion

It is not particularly uncommon for children to present with or to be evaluated for ovarian masses, and most of these are

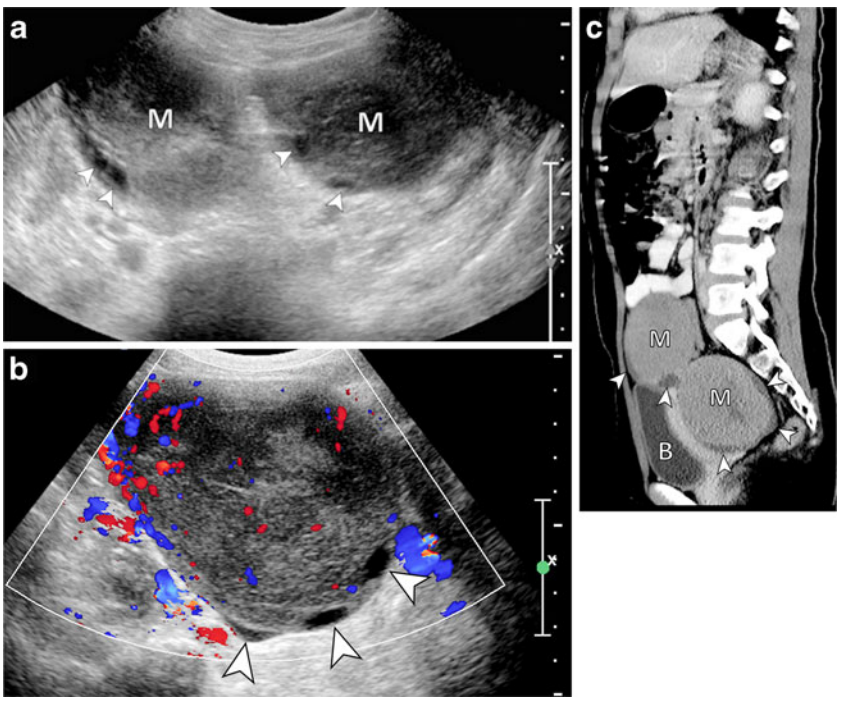

Fig. 18 A large retropharyngeal mass (image not shown) and bilateral ovarian masses in an 11-year-old girl who had a heart transplant at 9 months of age. **a** Transverse US scan through the pelvis shows bilateral, mildly heterogeneous and large pelvic adnexal masses (*M*) with small, peripheral cysts (*arrowheads*). **b** Color Doppler US demonstrates increased flow to the lesions and small peripheral cysts (*arrowheads*). **c** Sagittal reformatted contrast-enhanced CT image shows the two masses (*M*), one within the Douglas pouch and the second extending into the lower abdomen. Both lesions are mildly heterogeneous with small, peripheral cysts (*arrowheads*). Biopsy of the retropharyngeal mass was performed and the pathological assessment was consistent with Burkitt lymphoma, with positive in situ hybridization for Epstein-Barr virus confirming the expected diagnosis of post-transplant lymphoproliferative disorder. *B* = bladder

benign and represent simple or complex cysts, ovarian torsion or benign neoplasms [5, 7, 13]. US is the imaging modality of choice for visualizing the reproductive system in the pediatric population, particularly for the initial work–up, whereas CT and MRI are useful for tumor staging and follow-up. Mature teratomas are the most common benign ovarian tumors in children and adolescents, and although their cross-sectional imaging appearance is pathognomonic, their US appearance is quite variable, which is related to the presence of varying amounts of fat, calcific and cystic components [25, 26, 31, 33, 35]. A malignant ovarian lesion should be suspected in patients with lesions larger than 7.5–8.0 cm, lesions with predominantly solid components and in 1- to 8-year-old patients, particularly in those presenting with an abdominal mass or precocious puberty [7, 14, 19].

References

1. Piver MS, Patton T (1986) Ovarian cancer in children. Semin Surg Oncol 2:163–169
2. Brown MF, Hebra A, McGeehin K et al (1993) Ovarian masses in children: a review of 91 cases of malignant and benign masses. J Pediatr Surg 28:930–932
3. Brookfield KF, Cheung MC, Koniaris LG et al (2009) A population-based analysis of 1,037 malignant ovarian tumors in the pediatric population. J Surg Res 156:45–49
4. von Allmen D (2005) Malignant lesions of the ovary in childhood. Semin Pediatr Surg 14:100–105
5. Pomeranz AJ, Sabnis S (2004) Misdiagnoses of ovarian masses in children and adolescents. Pediatr Emerg Care 20:172–174
6. Morowitz M, Huff D, von Allmen D (2003) Epithelial ovarian tumors in children: a retrospective analysis. J Pediatr Surg 38:331–335
7. Oltmann SC, Garcia N, Barber R et al (2010) Can we preoperatively risk stratify ovarian masses for malignancy? J Pediatr Surg 45:130–134
8. Oltmann SC, Garcia NM, Barber R et al (2010) Pediatric ovarian malignancies: how efficacious are current staging practices? J Pediatr Surg 45:1096–1102
9. Quirk JT, Natarajan N (2005) Ovarian cancer incidence in the United States, 1992–1999. Gynecol Oncol 97:519–523
10. Quirk JT, Natarajan N, Mettlin CJ (2005) Age-specific ovarian cancer incidence rate patterns in the United States. Gynecol Oncol 99:248–250
11. Koulouris CR, Penson RT (2009) Ovarian stromal and germ cell tumors. Semin Oncol 36:126–136
12. Oltmann SC, Fischer A, Barber R et al (2010) Pediatric ovarian malignancy presenting as ovarian torsion: incidence and relevance. J Pediatr Surg 45:135–139
13. Cass DL, Hawkins E, Brandt ML et al (2001) Surgery for ovarian masses in infants, children, and adolescents: 102 consecutive patients treated in a 15-year period. J Pediatr Surg 36:693–699
14. Hayes-Jordan A (2005) Surgical management of the incidentally identified ovarian mass. Semin Pediatr Surg 14:106–110
15. Patterson DM, Rustin GJ (2006) Controversies in the management of germ cell tumours of the ovary. Curr Opin Oncol 18:500–506
16. Salonen JT, Uimari P, Aalto JM et al (2007) Type 2 diabetes whole-genome association study in four populations: the DiaGen consortium. Am J Hum Genet 81:338–345
17. Sheiko MC, Hart WR (1982) Ovarian germinoma (dysgerminoma) with elevated serum lactic dehydrogenase: case report and review of literature. Cancer 49:994–998
18. Stevens SK, Hricak H, Stern JL (1991) Ovarian lesions: detection and characterization with gadolinium-enhanced MR imaging at 1.5 T. Radiology 181:481–488
19. Vaysse C, Delsol M, Carfagna L et al (2010) Ovarian germ cell tumors in children. Management, survival and ovarian prognosis. A report of 75 cases. J Pediatr Surg 45:1484–1490
20. Panteli C, Curry J, Kiely E et al (2009) Ovarian germ cell tumours: a 17-year study in a single unit. Eur J Pediatr Surg 19:96–100
21. Pectasides D, Pectasides E, Kassanos D (2008) Germ cell tumors of the ovary. Cancer Treat Rev 34:427–441
22. Smith HO, Berwick M, Verschraegen CF et al (2006) Incidence and survival rates for female malignant germ cell tumors. Obstet Gynecol 107:1075–1085
23. Stranzinger E, Strouse PJ (2008) Ultrasound of the pediatric female pelvis. Semin Ultrasound CT MR 29:98–113
24. Cools M, Looijenga LH, Wolffenbuttel KP et al (2009) Disorders of sex development: update on the genetic background, terminology and risk for the development of germ cell tumors. World J Pediatr 5:93–102
25. Outwater EK, Siegelman ES, Hunt JL (2001) Ovarian teratomas: tumor types and imaging characteristics. Radiographics 21:475–490
26. Sheth S, Fishman E, Buck J et al (1988) The variable sonographic appearances of ovarian teratomas: correlation with CT. AJR 151:331–334
27. Beller MJ (1998) The “tip of the iceberg” sign. Radiology 209:395–396
28. Choudhary S, Fasih N, McInnes M et al (2009) Imaging of ovarian teratomas: appearances and complications. J Med Imaging Radiat Oncol 53:480–488
29. Servaes S, Victoria T, Lovrenski J et al (2010) Contemporary pediatric gynecologic imaging. Semin Ultrasound CT MR 31:116–140
30. Saba L, Guerriero S, Sulcis R et al (2009) Mature and immature ovarian teratomas: CT, US and MR imaging characteristics. Eur J Radiol 72:454–463
31. Surratt JT, Siegel MJ (1991) Imaging of pediatric ovarian masses. Radiographics 11:533–548
32. Park SB, Kim JK, Kim KR et al (2008) Imaging findings of complications and unusual manifestations of ovarian teratomas. Radiographics 28:969–983
33. Guinet C, Ghossain MA, Buy JN et al (1995) Mature cystic teratomas of the ovary: CT and MR findings. Eur J Radiol 20:137–143
34. Shanbhogue AK, Shanbhogue DK, Prasad SR et al (2010) Clinical syndromes associated with ovarian neoplasms: a comprehensive review. Radiographics 30:903–919
35. Alotaibi MO, Navarro OM (2010) Imaging of ovarian teratomas in children: a 9-year review. Can Assoc Radiol J 61:23–28
36. Nimkin K, Gupta P, McCauley R et al (2004) The growing teratoma syndrome. Pediatr Radiol 34:259–262
37. Postovsky S, Epelbaum M, Ben Itzhak O et al (2004) Growing teratoma syndrome treated by interferon alpha-2beta: case report and literature review. Pediatr Hematol Oncol 21:9–16
38. Tanaka YO, Kurosaki Y, Nishida M et al (1994) Ovarian dysgerminoma: MR and CT appearance. J Comput Assist Tomogr 18:443–448
39. Outwater EK, Wagner BJ, Mannion C et al (1998) Sex cord-stromal and steroid cell tumors of the ovary. Radiographics 18:1523–1546
40. Cecchetto G, Ferrari A, Bernini G et al (2011) Sex cord stromal tumors of the ovary in children: a clinicopathological report from the Italian TREP project. Pediatr Blood Cancer 56(7):1062–1067
41. Young RH, Dickersin GR, Scully RE (1984) Juvenile granulosa cell tumor of the ovary. A clinicopathological analysis of 125 cases. Am J Surg Pathol 8:575–596

42. Pectasides D, Pectasides E, Psyrri A (2008) Granulosa cell tumor of the ovary. Cancer Treat Rev 34:1–12
43. Tanaka YO, Saida TS, Minami R et al (2007) MR findings of ovarian tumors with hormonal activity, with emphasis on tumors other than sex cord-stromal tumors. Eur J Radiol 62:317–327
44. Tanaka YO, Tsunoda H, Kitagawa Y et al (2004) Functioning ovarian tumors: direct and indirect findings at MR imaging. Radiographics 24(Suppl 1):S147–166
45. Jung SE, Rha SE, Lee JM et al (2005) CT and MRI findings of sex cord-stromal tumor of the ovary. AJR 185:207–215
46. Kim SH, Kim SH (2002) Granulosa cell tumor of the ovary: common findings and unusual appearances on CT and MR. J Comput Assist Tomogr 26:756–761
47. Morikawa K, Hatabu H, Togashi K et al (1997) Granulosa cell tumor of the ovary: MR findings. J Comput Assist Tomogr 21:1001–1004
48. Imaoka I, Wada A, Kaji Y et al (2006) Developing an MR imaging strategy for diagnosis of ovarian masses. Radiographics 26:1431–1448
49. Mak CW, Tzeng WS, Chen CY (2009) Computed tomography appearance of ovarian fibrothecomas with and without torsion. Acta Radiol 50:570–575
50. Swanger RS, Brudnicki A (2007) Ultrasound of ovarian sex-cord tumor with annular tubules. Pediatr Radiol 37:1270–1271
51. Shen K, Wu P-C, Lang J-H et al (1993) Ovarian sex cord tumor with annular tubules: a report of six cases. Gynecol Oncol 48:180–184
52. Bercaw JL, Sanchez J, Byrd RH et al (2010) Sex cord tumor with annular tubules in a young adolescent with Von Willebrand's disease. J Pediatr Adolesc Gynecol 23:e111–e114
53. Iyer VR, Lee SI (2010) MRI, CT, and PET/CT for ovarian cancer detection and adnexal lesion characterization. AJR 194:311–321
54. Massicot R, Rousseau V, Darwish AA et al (2009) Serous and seromucinous infantile ovarian cystadenomas—a study of 42 cases. Eur J Obstet Gynecol Reprod Biol 142:64–67
55. Jung SE, Lee JM, Rha SE et al (2002) CT and MR imaging of ovarian tumors with emphasis on differential diagnosis. Radiographics 22:1305–1325
56. Sri Paran T, Mortell A, Devaney D et al (2006) Mucinous cystadenoma of the ovary in perimenarchal girls. Pediatr Surg Int 22:224–227
57. Outwater EK, Siegelman ES, Talerman A et al (1997) Ovarian fibromas and cystadenofibromas: MRI features of the fibrous component. J Magn Reson Imaging 7:465–471
58. Cho SM, Byun JY, Rha SE et al (2004) CT and MRI findings of cystadenofibromas of the ovary. Eur Radiol 14:798–804
59. Young RH, Oliva E, Scully RE (1994) Small cell carcinoma of the ovary, hypercalcemic type. A clinicopathological analysis of 150 cases. Am J Surg Pathol 18:1102–1116
60. Young RH, Oliva E, Scully RE (1995) Small cell carcinoma of the hypercalcemic type in the ovary. Gynecol Oncol 57:7–8
61. Scully RE (1993) Small cell carcinoma of hypercalcemic type. Int J Gynecol Pathol 12:148–152
62. Isonishi S, Nishii H, Saitou M et al (2008) Small cell carcinoma of the ovary: clinical and biological study. Int J Clin Oncol 13:161–165
63. McCarville MB, Hill DA, Miller BE et al (2001) Secondary ovarian neoplasms in children: imaging features with histopathologic correlation. Pediatr Radiol 31:358–364
64. Crawshaw J, Sohaib SA, Wotherspoon A et al (2007) Primary non-Hodgkin's lymphoma of the ovaries: imaging findings. Br J Radiol 80:e155–158
65. Koukourgianni F, Harambat J, Ranchin B et al (2010) Malignancy incidence after renal transplantation in children: a 20-year single-centre experience. Nephrol Dial Transplant 25:611–616